A Highly Reversible Zinc Anode for Rechargeable Aqueous Batteries

Qinping Jian [a,b,1], Yuhan Wan [a,b,1], Yanke Lin [a,b], Meng Ni [c,d], Maochun Wu [a,b,*], Tianshou Zhao [a,b,**]

[a] *Department of Mechanical and Aerospace Engineering, The Hong Kong University of Science and Technology, Clear Water Bay, Kowloon, Hong Kong SAR 999077, China*

[b] *HKUST Energy Institute, The Hong Kong University of Science and Technology, Clear Water Bay, Kowloon, Hong Kong SAR 999077, China*

[c] *Department of Building and Real Estate, The Hong Kong Polytechnic University, Hung Hom, Kowloon, Hong Kong SAR 999077, China*

[d] *Environmental Energy Research Group, Research Institute for Sustainable Urban Development, The Hong Kong Polytechnic University, Hung Hom, Kowloon, Hong Kong SAR 999077, China*

Abstract

Zinc metal holds a great potential as an anode material for next-generation aqueous batteries due to its suitable redox potential, high specific capacity, and low cost. However, the uncontrollable dendrite growth and detrimental side reactions with electrolytes hinder the practical application of this type of electrode. To tackle the issues, an ultra-thin (~1 μm) sulfonated poly(ether ether ketone) (SPEEK) solid-electrolyte interphase (SEI) is constructed onto the Zn anode surface by a facile spin-coating method. We demonstrate that the polymeric SEI simultaneously blocks the water molecules and anions, uniformizes the ion flux, and facilitates the de-solvation process of Zn^{2+} ions, thus effectively suppressing the side reactions

[1] Q.P. Jian and Y.H. Wan contributed equally to this work.

[*] Corresponding author. E-mail: mwuah@connect.ust.hk (M.C. Wu).

[**] Corresponding author. E-mail: mwuah@connect.ust.hk (T.S. Zhao).

and Zn dendrite formation. As a result, the newly developed Zn@SPEEK anode enables a symmetric cell to stably operate over 1000 cycles at 5 mA cm^{-2} without degradation. Moreover, with the Zn anode paired with a MnO_2 cathode, the full cell exhibits an improved coulombic efficiency (over 99% at 0.1 A g^{-1}), a superior rate capability (127 mAh g^{-1} at 2 A g^{-1}), and excellent cycling stability (capacity retention of 70% over 1000 cycles at 1 A g^{-1}). This work provides a facile yet effective strategy to address the critical challenges in Zn anodes, paving the way for the development of high-performance rechargeable aqueous batteries.

Keywords: Zinc metal anode; Solid-electrolyte interphase; Dendrite-free; Anti-corrosion; Rechargeable aqueous batteries

1. Introduction

The widespread adoption of renewable energies (e.g., solar and wind) requires efficient and economical grid-scale energy storage technologies to ensure stable power output[1,2]. Rechargeable batteries are regarded as one of the most promising candidates for this application, owing to the merits of high energy efficiency, good site-independency, and excellent scalability[3,4]. Among various candidates, rechargeable aqueous batteries are especially attractive because of their unique advantages, including high safety, high power capability, low cost, and environmental friendliness[5–9]. Particularly, aqueous zinc (Zn) metal batteries have gained enormous research interest owing to the outstanding properties of Zn anode, which has a high theoretical capacity (820 mAh g^{-1} and 5855 mAh cm^{-3}), favorable redox potential (−0.76 V vs. standard hydrogen electrode), and good stability in aqueous environment[10–12]. Although great progress has been made in several types of aqueous Zn batteries (e.g., Zn-Ni and Zn–air

battery) over the past several decades[13,14], state-of-the-art rechargeable Zn batteries employing alkaline electrolytes are still confronted with some insurmountable challenges, such as severe side reactions, including hydrogen evolution reactions and surface passivation, shape change, and dendrite growth[15–17]. Recently, it is found that using a mild/neutral electrolyte in Zn batteries could mitigate the problems of Zn electrode to some extent, which has thereby aroused enormous research interest in these systems[18–21]. However, dendrite growth and side reactions with electrolytes still exist in mildly acidic aqueous electrolytes, which contribute to the poor cyclability, low efficiency and even short-circuit-induced failure of aqueous Zn batteries[22,23].

Over the past decade, extensive research has been conducted to address the aforementioned issues of Zn anodes, including functional nucleation regulations[24–26], 3D electrode engineering[27–32], surface manipulation[33–38], separator design[39,40], concentrated electrolytes[41–43], and electrolyte additives[44–46]. Among them, manipulating the Zn/electrolyte interface is considered as one of the most promising ways to improve the Zn anode, because it could conveniently regulate the ion transfer, solvent and electric field distribution at the interface, which plays a determining role in the reversibility and uniformity of Zn plating/stripping behavior. Thus far, various materials and methods have been applied to construct a functional protective layer or artificial solid-electrolyte interphase (SEI) on Zn anode, including inorganic metal oxides and elastic polymers. For instance, porous layers comprising inorganic mineral particles (e.g., $CaCO_3$ and ZrO_2) were employed to regulate the ion flux at the Zn/electrolyte interface, thus inhibiting dendrite formation[35,47]. Unfortunately, such porous layers were water permeable and lack of effective cation selectivity, rendering

them incapability of terminating the detrimental side reactions induced by aqueous electrolytes. To address this issue, thin, dense metal oxides (e.g., Al_2O_3 and TiO_2) layers were coated on the surface of Zn metal anode using the atomic layer deposition technique[34,36]. Although these layers could protect Zn anodes from side reactions, the inhibition effect was rather limited, possibly due to the low selectivity of ion and water as well as the poor mechanical strength which may easily cause breakage during repeated plating/stripping cycles. Alternatively, elastic polymers with enhanced mechanical properties, such as polyamide[48], commercial cyanoacrylate glue[49] and Nafion[50], were investigated as coating materials to improve the electrochemical performance of Zn anode. Unfortunately, these polymers cannot meet the stringent requirements for an ideal SEI, which needs to have a high ionic conductivity and selectivity, good mechanical strength, and excellent stability in the aqueous electrolyte. In addition, the SEI should be as thin as possible to minimize the sacrifice of energy density and internal resistance while able to suppress the side reactions and dendrite growth effectively.

In this work, an ultra-thin (~1 μm) yet mechanically strong sulfonated poly(ether ether ketone) (SPEEK) layer is spin-coated on the Zn metal surface as a de-solvation and anion-blocking SEI to simultaneously address the both issues. As schematically illustrated in Figure 1, the thin, uniform coating of cation selective SPEEK SEI with proper ion channel size could effectively prevent the anions and de-solvated water molecules from contacting the Zn surface and facilitate de-solvations of Zn^{2+} ions with functional sulfonic acid groups[51,52], thus significantly restraining the side reactions. In addition, the polymer film shows good adhesion to the Zn surface, high mechanical strength and improved hydrophilicity, which effectively

constrains lateral ion diffusion and render homogenous ion distribution on the Zn surface, thus enabling uniform Zn deposition/dissolution underneath the artificial SEI layer. Consequently, the SPEEK protected Zn electrode (Zn@SPEEK) delivers a considerably extended cycle life of 500 h in a symmetric cell at 5 mA cm^{-2}. More impressively, a Zn@SPEEK||MnO_2 full battery shows excellent cycling stability with an improved coulombic efficiency (CE) of 99.2% at 0.1 A g^{-1} and an outstanding capacity retention rate of 70% at 1 A g^{-1} over 1000 cycles, far surpassing that with the unprotected Zn electrode, which exhibits a CE of 97% at 0.1 A g^{-1} and can only retain 34% of its initial capacity after 1000 cycles at 1 A g^{-1}.

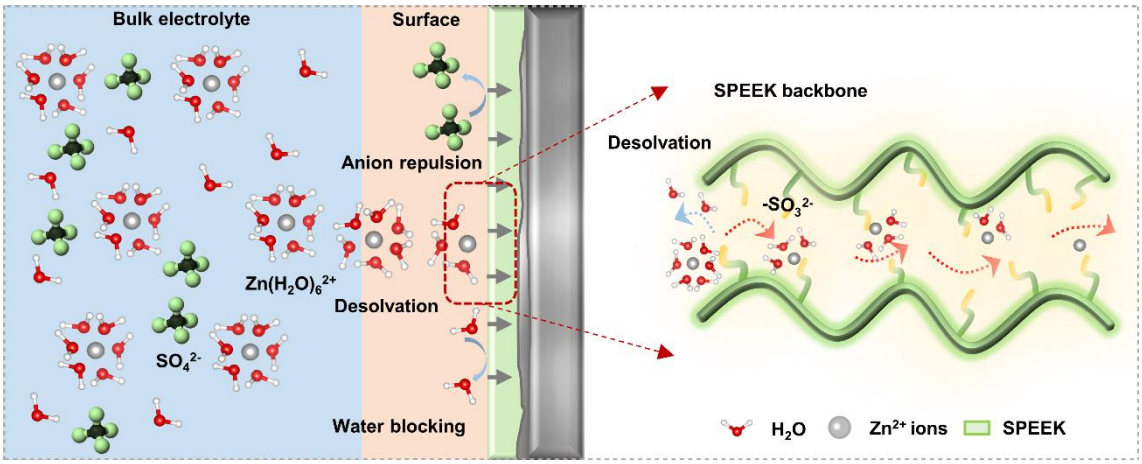

Figure 1. Schematic illustrations of SPEEK SEI on the Zn surface, which facilitates de-solvation of Zn^{2+} ions, blocks water molecules and repels anions during deposition.

2. Results and discussion

The fabrication process of SPEEK SEI on the Zn anode is illustrated in Figure 2a. First, the as-prepared SPEEK solution is dropped onto the Zn foil surface and after a simple spin-coating process, the SPEEK solution uniformly covers the Zn surface and forms a SPEEK film after evaporation of the solvent. The morphology of Zn@SPEEK SEI was first studied by scanning electron microscope (SEM). As displayed in Figure 2b, the SPEEK film is dense and uniform with a thickness of ~1 μm, which is determined by the cross-sectional image with energy dispersive spectroscopy (EDS) mappings (Figure 2c). Figure 2d displays the Fourier-transform infrared spectroscopy (FTIR) of SPEEK SEI film, which exhibits several characteristic peaks. The absorption peaks at around 1086 and 1220 cm^{-1} are ascribed to the asymmetric and symmetric stretching vibrations of O=S=O bonds, while that located at 1027 cm^{-1} is attributed to S-O bonds, confirming the successful synthesis of SPEEK with functional sulfonic acid groups[53–55]. The X-ray diffraction (XRD) patterns in Figure 2e reveals a broad peak of SPEEK, which can barely be detected in the Zn@SPEEK, indicating that it is mainly amorphous and

the coating layer is ultra-thin. In addition, rolling experiment (Figure S1, Supporting Information) was performed to investigate the adhesion strength between the SPEEK layer and Zn foil. It is shown that even after rolling, the SPEEK SEI is still tightly attached on the Zn surface, indicating the strong adhesion of SPEEK layer to Zn anode. The hydrophilicity of the SPEEK was evaluated by measuring the contact angle at ambient temperature (25 °C). As displayed in Figure S2a, the bare Zn exhibits a contact angle of about 86.1°, suggesting the poor hydrophilicity of the pristine Zn metal surface toward aqueous solution. By comparison, Zn@SPEEK displays a contact angle of 62.4° (Figure S2b), indicating the hydrophilicity is improved in the presence of SPEEK polymeric layer with hydrophilic sulfonic acid groups, which can reduce the interfacial free energy between the electrolyte and Zn anode[56,57], thereby contributing to a homogeneous ion flux at the Zn/electrolyte interface and thus uniform Zn plating and stripping.

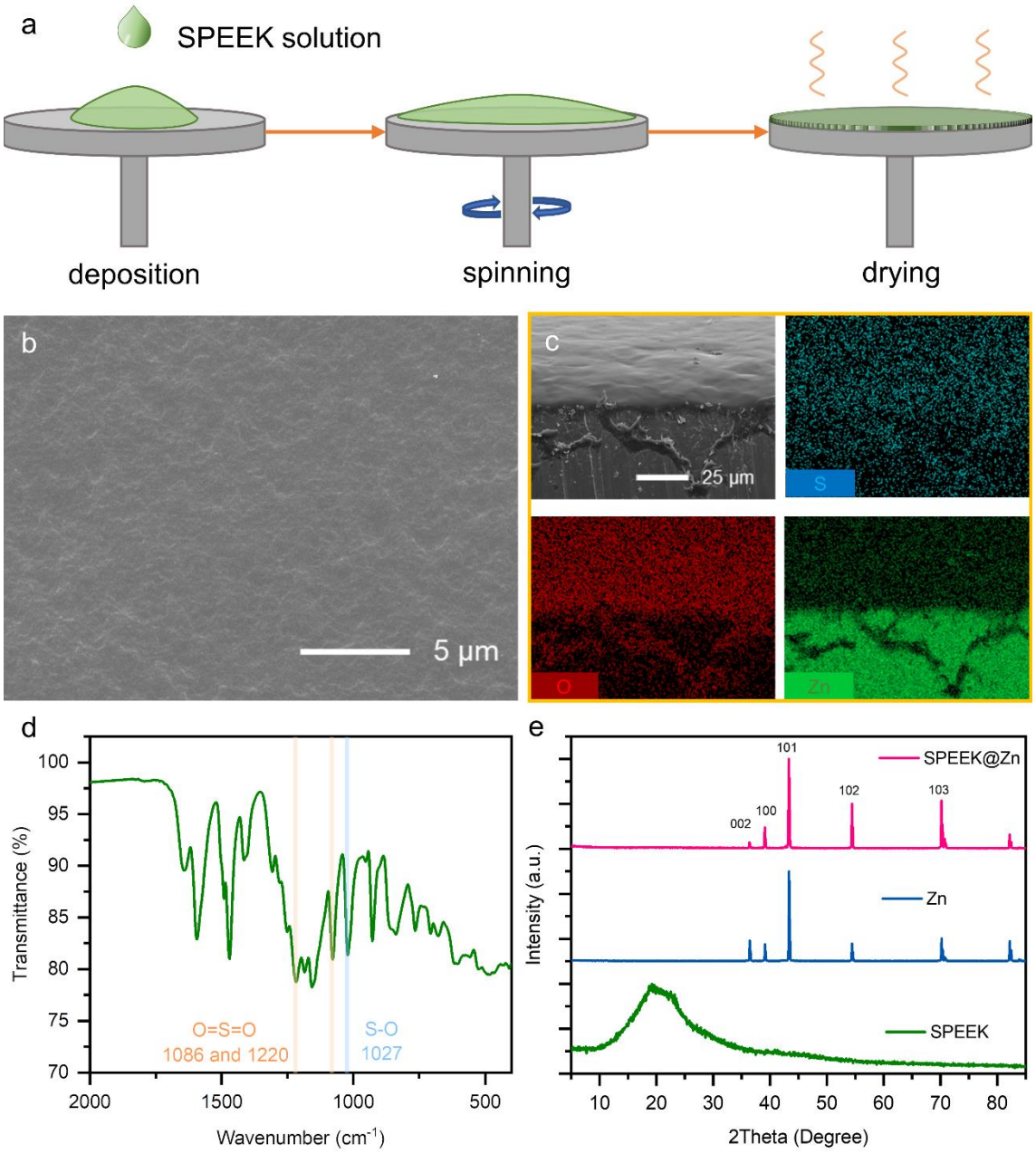

Figure 2. (a) Schematic illustration of spin coating process for preparing SPEEK SEI on the Zn surface. (b) SEM image of the Zn@SPEEK surface. (c) Cross-sectional SEM image of Zn@SPEEK with EDS mappings of S, O, and Zn elements, respectively. (d) FTIR spectrum of SPEEK film. (e) XRD patterns of bare Zn foil, Zn@SPEEK, and SPEEK film.

The effect of SPEEK on the electrochemical behaviors of Zn anode was first investigated by cyclic voltammetry (CV) tests. As displayed in Figure 3a, typical Zn deposition and dissolution peaks are clearly seen on both Cu and Cu@SPEEK substrates. The ratio of cathodic and anodic current density on the Cu@SPEEK substrate is improved compared to the bare Cu, suggesting the reversibility of Zn plating/stripping process is enhanced in the presence of SPEEK SEI. To analyze the effect of SPEEK SEI on suppressing the side reactions of Zn anode, corrosion current densities were measured with linear polarization curves using Tafel linear extrapolation in a three-electrode cell. As can be seen in Figure 3b, Zn@SPEEK shows a low corrosion current density of 2.4 mA cm^{-2}, in comparison to 5.4 mA cm^{-2} of the bare Zn foil in the same electrolyte, indicating that the Zn corrosion in aqueous electrolyte is significantly inhibited with the protection of SPEEK SEI. The protection ability of the SPEEK layer was further evaluated by immersing Zn@SPEEK in 1 M $ZnSO_4$ for one week and compared to the bare Zn electrode under the same conditions. As presented in Figure S3a, the surface of bare Zn foil changes from silver white to dark gray and the SEM image shows that the Zn surface is covered by a layer of porous by-products, implying the severe side reactions between Zn and electrolyte. In striking contrast, the Zn@SPEEK electrode maintains the metal luster even after 7-day immersion (Figure S3b), indicating Zn corrosion from the electrolyte is successfully prevented by the SPEEK. SEM image of Zn@SPEEK after corrosion further shows that the Zn surface maintains smooth and no obvious by-product crystals are found. XRD patterns of different Zn anodes after corrosion are shown in Figure S3c. Three characteristic peaks at 8.1, 16.2 and 24.4° in the XPD pattern of the bare Zn after corrosion test are detected, which are

attributed to $Zn_4SO_4(OH)_6 \cdot 5H_2O$, a main by-product of side reactions in 1 M $ZnSO_4$ solution[56,58]. By comparison, there are no evident peaks of the by-products on Zn@SPEEK, which further demonstrates the effectiveness of the SPEEK SEI in blocking the anions and water molecules, thus suppressing the side reactions in the aqueous electrolyte.

Chronoamperometry (CA) was adopted to investigate the nucleation and following growth of Zn deposition at a constant overpotential, as the variation of current with respect to time is able to susceptibly reflects the change in surface area/roughness during deposition process[59]. The chronoamperograms of different Zn electrodes are compared in Figure 3c. At a constant overpotential of −150 mV vs. Zn/Zn^{2+}, the deposition current density of bare Zn electrode increases monotonically within the whole period of 300 s. The continuous rise in current density indicates the increase of true surface area, which originates from the dendritic Zn deposition. By contrast, the transient current of the Zn@SPEEK electrode increases in the early stage (within 50 s) and then remains stable till the end of the deposition, suggesting a relatively smooth Zn surface without obvious dendrite formation during the Zn deposition. Previous studies have shown that, on a bare Zn anode, the Zn ions adsorbed on the surface tend to diffuse laterally and aggregate to form initial nuclei as a result of minimizing surface energy during the nucleation process[59,60]. The continuous lateral diffusion of adsorbed Zn^{2+} ions and concentrated electric field near the tips of protuberances will amplify the nuclei into severe dendrites, as schematically illustrated in Figure S4a. In contrast, the presence of SPEEK SEI will constrain the lateral diffusion of Zn^{2+} ions, leading to the formation of more uniform and finer nucleus seeds in the early stage. Moreover, the SPEEK layer on the vicinity of the initial

protuberances of the Zn nuclei will homogenize the ion distribution in the following deposition, which will inhibit Zn^{2+} ions from accumulating and being reduced on these nuclei (Figure S4b). As a consequence, the constrained lateral diffusion of Zn^{2+} ions and suppressed tip effect collectively lead to uniform, dendrite-free Zn deposition.

The ion transference and de-solvation kinetics of Zn^{2+} ions at different electrode/electrolyte interfaces were investigated by measuring the activation energy (E_a) of Zn deposition. As shown in Figure 3d and e, the charge transfer resistance (R_{ct}) of bare Zn is larger than that of Zn@SPEEK at different temperatures, indicating a lower energy barrier for Zn^{2+} ion transfer and de-solvation on the SPEEK interface. The activation energy of Zn@SPEEK is calculated to be only 45.0 kJ mol^{-1} (Figure 3f), compared to 57.8 kJ mol^{-1} of bare Zn, indicating that the improved Zn deposition on Zn@SPEEK is mainly attributed to the facilitated de-solvation kinetics enabled by the strong interaction between solvated Zn^{2+} ions and sulfonic acid groups[50,61–63]. Moreover, the SPEEK SEI features an ionic conductivity of as high as 1.98 mS cm^{-1} in $ZnSO_4$ solution (Figure S5), which allows fast Zn^{2+} ion transport through this protective layer. The transference number of Zn^{2+} ion (t_{Zn}) was further measured to evaluate the selectivity of the SPEEK layer. As shown Figure S6a, the t_{Zn} is determined to be 0.19 in the bare Zn symmetric cell, which is consistent with previous results[64,65]. The low value of t_{Zn} mainly originates from the faster migration of anions than solvated Zn^{2+} ions[56]. After introducing the ultra-thin cation-selective SPEEK SEI on the Zn surface, the t_{Zn} is dramatically improved to 0.49 (Figure S6b), owing to the negatively charged sulfate groups in SPEEK, which provide pathways for Zn^{2+} ion transfer while effectively block anions from

diffusing through the SPEEK. The high ionic conductivity and selectivity of SPEEK SEI could reduce the concentration gradient and facilitate uniform distribution of Zn^{2+} ions, thus contributing to homogeneous Zn deposition without dendrite formation.

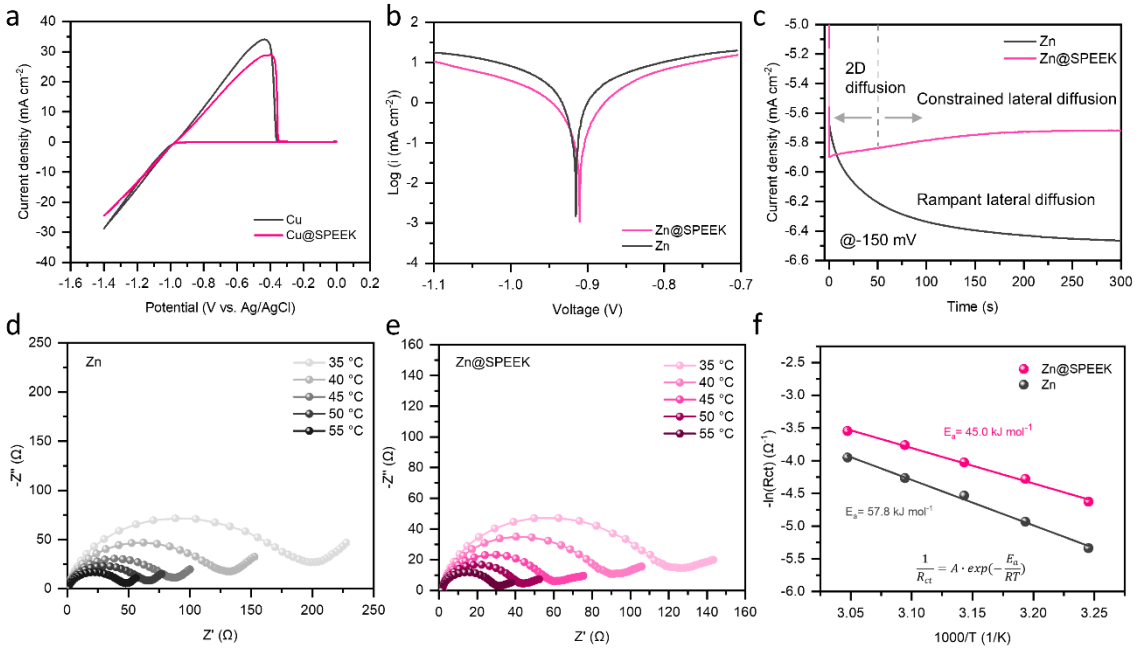

Figure 3. (a) CV curves of Zn plating and stripping on Cu and Cu@SPEEK substrates. (b) Tafel curves of Zn and Zn@SPEEK. (c) Chronoamperograms of Zn deposition on bare Zn and Zn@SPEEK anodes. Nyquist plots of (d) Zn and (e) Zn@SPEEK symmetric cells at different temperatures. (f) Arrhenius curves of activation energy of Zn and Zn@SPEEK.

To investigate the effect of SPEEK SEI on Zn dendrite inhibition, an operando optical observation system was constructed to in situ monitor the Zn plating behavior. As shown in Figure 4a, the special configuration of the cell provides a transparent window through which the microscope and camera could in-situ observe and record the morphology evolution of the deposited Zn. The Zn deposition was conducted at 2 mA cm^{-2} with an areal capacity of 5 mAh cm^{-2}. As displayed in Video S1, uneven Zn nucleation and obvious dendrite growth appear on the pristine Zn electrode in the $ZnSO_4$ electrolyte. Figure 4b1-4b5 show the snapshots with

different capacity of Zn deposited on the bare Zn substrate. After a plating capacity of 0.1 mAh cm^{-2}, an uneven nucleation distribution starts on the Zn electrode surface. With further plating, protrusions gradually form on the surface and evolve into obvious Zn dendrites. The in-situ observation confirms that the inhomogeneous nucleation and dendritic Zn deposition on bare Zn easily occur in 1 M $ZnSO_4$ electrolyte because of the free lateral diffusion of ions and tip effects. Consequently, the formation of Zn dendrites results in the poor reversibility of bare Zn electrodes during the repeated cycles. By comparison, Zn plating on the Zn@SPEEK electrode is homogeneous and exhibits a smooth morphology (Video S2). No Zn dendrites are found after 5 mAh cm^{-2} of Zn is plated on Zn@SPEEK electrode, as evidenced in Figure 4c1-c5. *Ex-situ* SEM images of the Zn morphologies further reveal the different deposition behavior on Zn and Zn@SPEEK electrodes. As shown in Figure 4d and e, the deposited Zn tends to nucleate sparsely and randomly on the bare Zn surface, which grows into dendrites towards the separator as seen from the cross-sectional view (Figure 4f). By contrast, Zn is uniformly deposited onto Zn@SPEEK electrode, showing a compact and flat surface after peeling off SPEEK SEI (Figure 4g and h). No obvious dendrite towards the separator is observed from the cross-sectional view in Figure 4i, which indicates a uniform and dendrite-free plating behavior with the assist of SPEEK SEI. To distinguish the superior effect of SPEEK on inhibiting Zn dendrite formation, Zn deposition on Nafion coating Zn electrode (Zn@Nafion) was investigated under the same experimental conditions. As shown in Figure S7, obvious Zn dendrites and penetration of Nafion film are observed by SEM after Zn deposition. To reveal difference of dendrite suppression capability, the mechanical strength of SPEEK and Nafion were measured

and compared using strain-stress curves (Figure S8). It is found that SPEEK presents a high young's modulus of 4.3 GPa, which is an order of magnitude higher than that of the Nafion polymer (0.4 GPa), indicating that a high mechanical strength is necessary for a robust SEI to withstand the high stress variation and the penetration force.

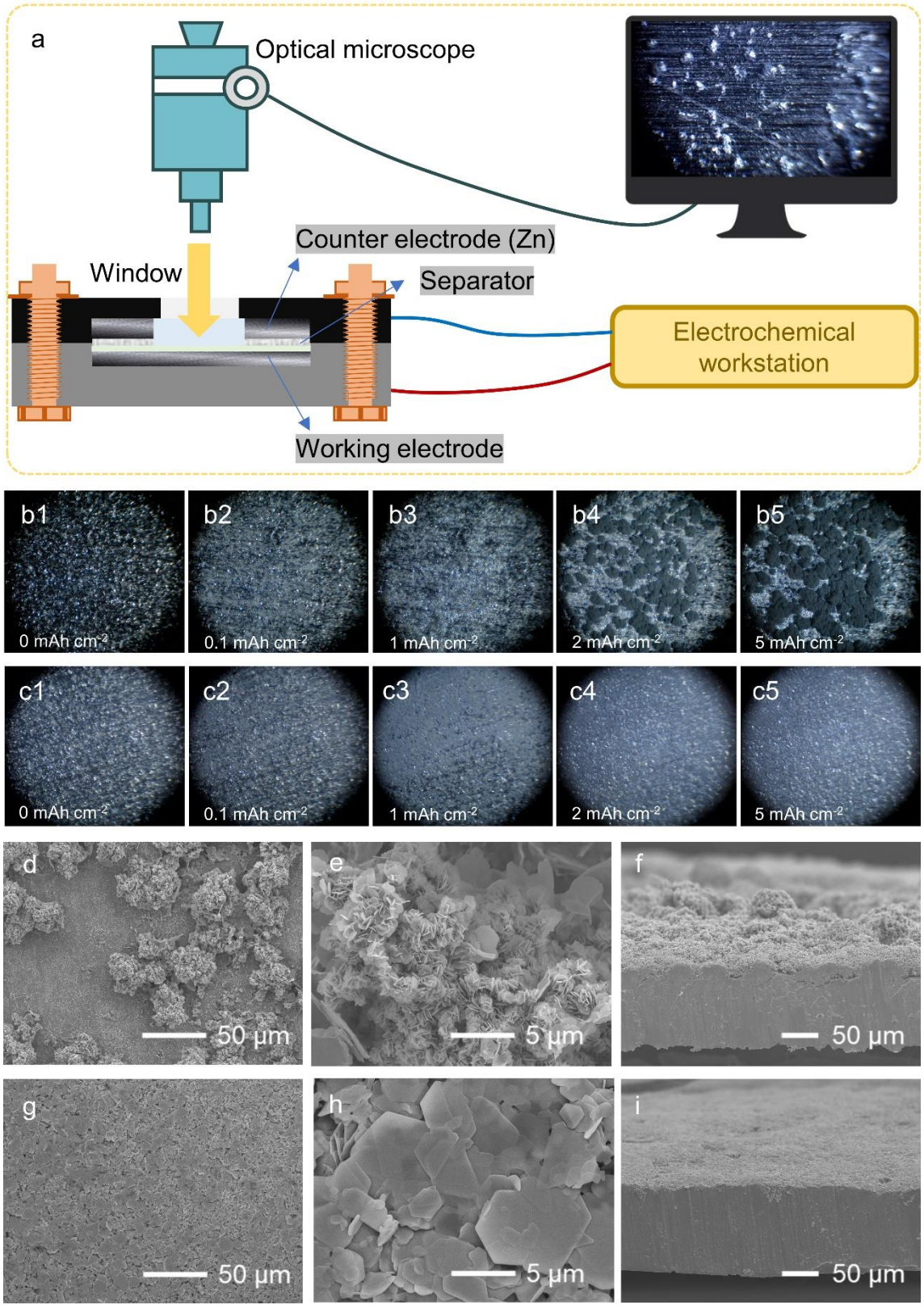

Figure 4. (a) Schematic of the in-situ optical microscope observation system for Zn deposition.

Morphology evolution of the Zn electrodeposits on (b1-b5) bare Zn and (c1-c5) Zn@SPEEK

anode. *Ex-situ* SEM images of Zn deposition on (d-f) bare Zn and (g-i) Zn@SPEEK (after peeling off SPEEK).

The superiority of the Zn@SPEEK electrode was further evaluated in asymmetric and symmetric cells by galvanostatic cycling. The 'reservoir half-cell' protocol was first adopted to assess the reversibility of Zn plating/stripping in an asymmetric cell, where Cu and Cu@SPEEK were employed as the working electrode and Zn foil as counter electrode[66,67]. As shown in Figure 5a and b, the asymmetric cells are first cycled with two charge/discharge cycles to dimmish other effects (e.g., alloy formation and different surface roughness) at 1 mA cm^{-2} with an areal capacity of 1 mAh cm^{-2} and a charge cut-off voltage of 1 V. 1 mAh cm^{-2} of Zn (Q_p) is subsequently electrodeposited onto the Cu or Cu@SPEEK working electrode as a Zn reservoir, followed by cycling at a fixed capacity of 0.2 mAh cm^{-2} (Q_c). After n cycles (n equals to 10 in this work), all removable Zn (Q_s) in the cells is fully stripped to a cut-off voltage of 1 V. The average CE can then be calculated by the equation $CE = (nQ_c + Q_s)/(nQ_c + Q_p)$. Results reveal that Cu@SPEEK displays much more stable plating/stripping performance and higher average CE than bare Cu (98.0% vs. 88.7%), indicating that the capacity loss of the Zn plating/stripping cycles originating from side reactions is considerably suppressed with the protection of SPEEK SEI. Symmetric cells with different Zn anodes were cycled at different current densities and areal capacities to further examine the cycling stability of the Zn@SPEEK electrode. As presented in Figure 5c, the cell equipped with the Zn@SPEEK electrode exhibits a much lower voltage hysteresis (31 mV) than that with the bare Zn electrode (52 mV) at 1 mA cm^{-2} and 1 mA h cm^{-2}. Moreover, the Zn@SPEEK electrode enables the cell to retain extremely

stable voltage polarizations over 450 h without a short circuit, while the cell with the pristine Zn electrode undergoes fluctuating polarizations and suffers from failure after less than 50 h. It should be noted that the cycle life of symmetric cell with bare zinc anode may vary because of the severe, uncontrollable dendrite formation and side reactions of bare Zn electrodes, as shown in Figure S9. When the current density is increased to 5 mA cm^{-2}, the cell with bare Zn electrode displays larger voltage hysteresis and becomes shorted after less than 25 h, whereas the cell with Zn@SPEEK is able to be cycled stably for over 400 h (1000 cycles) with lower voltage hysteresis at 5 mA cm^{-2} (Figure 5d). More remarkably, the cell equipped with the Zn@SPEEK electrode can still maintain a stable cycling performance over 450 h at a high areal capacity of 5 mAh cm^{-2}, outperforming most previously reported interfacial modification works (Table S1), whilst its unprotected counterpart suffers from internal short circuit only after around 30 h. The superior cycling performance of Zn@SPEEK symmetric cell further demonstrate that the SPEEK SEI is able to effectively alleviate the side reactions and Zn dendrite growth during the repeated plating/stripping cycles, thus dramatically prolonging the cycle life of Zn anodes.

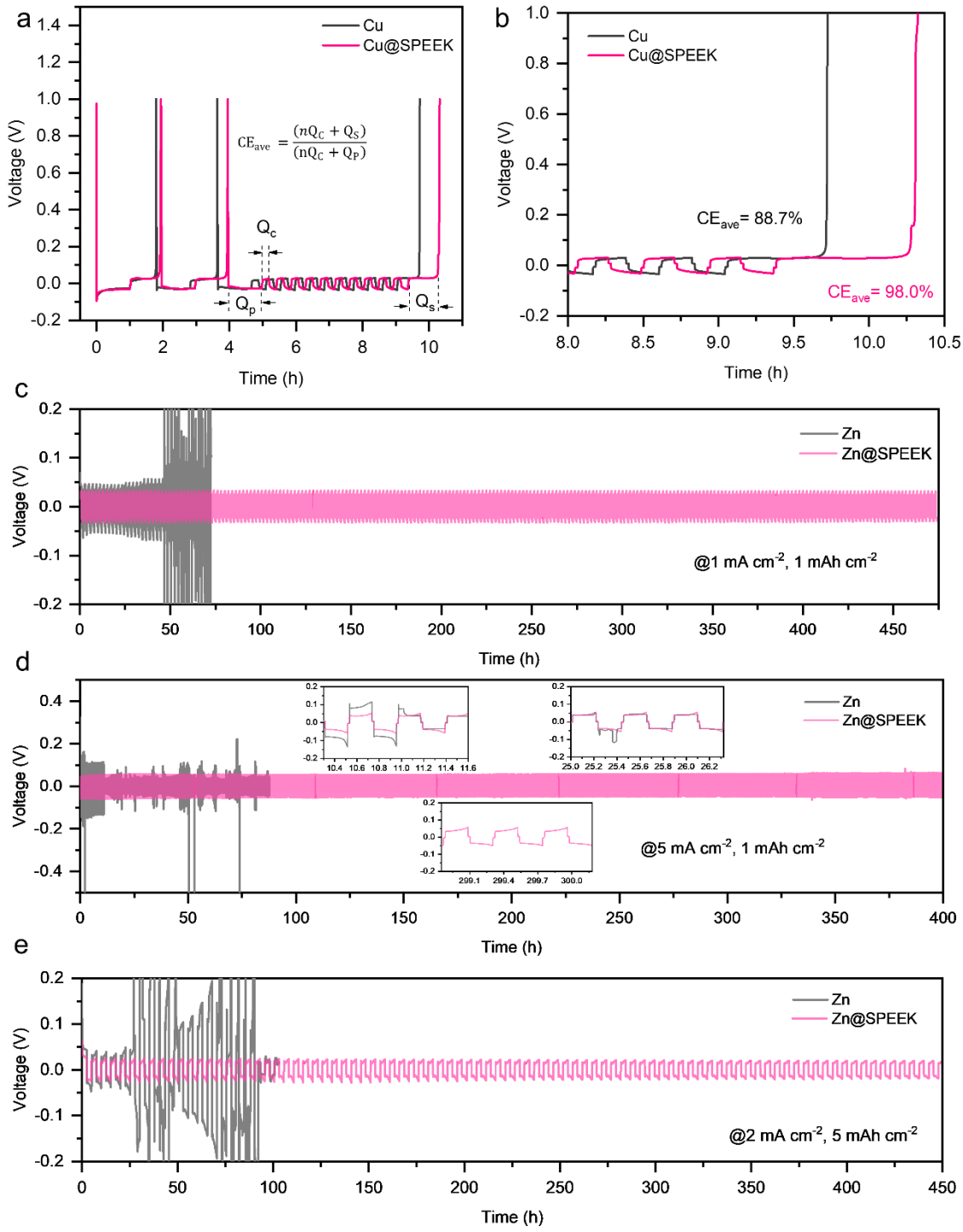

Figure 5. (a) CE test of Zn plating and stripping on Cu and Cu@SPEEK substrates for 10 cycles. (b) Comparison of fully stripping voltage profiles of Zn on Cu and Cu@SPEEK. Long-term galvanostatic cycling performance of symmetric Zn@SPEEK and Zn cells at a current density of (c) 1 and (d) 5 mA cm^{-2} with an areal capacity of 1 mA h cm^{-2} (Inset shows the corresponding

Zn plating/stripping curves after certain cycles), and (e) 2 mA cm^{-2} with an areal capacity of 5 mA h cm^{-2}.

Figure 6 compares the surface morphologies of the Zn@SPEEK and Zn electrode after 50 cycles in symmetric cells at 5 mA cm^{-2} and 1 mAh cm^{-2}. For the cycled bare Zn electrode, a rough surface covered with a large amount of flaky dendrites are evidently observed in Figure 6a and b, which results in the drastic fluctuations of the voltage polarization and final short circuit during the cycling. By comparison, as displayed in Figure 6c and d, the SPEEK SEI of the Zn@SPEEK electrode remains intact and shows no cracks or penetrations after cycles, indicating the outstanding durability of the SPEEK SEI and thus long-lasting protection effect for the Zn anode. The morphology of the deposited Zn surface was characterized by peeling off the SPEEK layer. As displayed in Figure 6e and f, Zn mainly deposits in the form of flakes that are parallel to the current collector and no vertical growth of Zn dendrites is observed under the SPEEK SEI, which contributes to the long-term stable cycling performance of the symmetric cell. Furthermore, as presented in the XRD patterns of cycled Zn anodes (Figure 6g), the characteristic peaks of $Zn_4SO_4(OH)_6 \cdot 5H_2O$ by-product located at 8.1, 16.2 and 24.4° are clearly detected on the bare Zn, which, by contrast, are barely detectable on the Zn@SPEEK surface after peeling off the SPEEK SEI, suggesting that the side reactions are significantly suppressed on Zn@SPEEK. Additionally, the peak of Zn (002) plane on the Zn@SPEEK shows a higher intensity than that on bare Zn anode, which implies more compact Zn deposition on the Zn@SPEEK electrode[68,69].

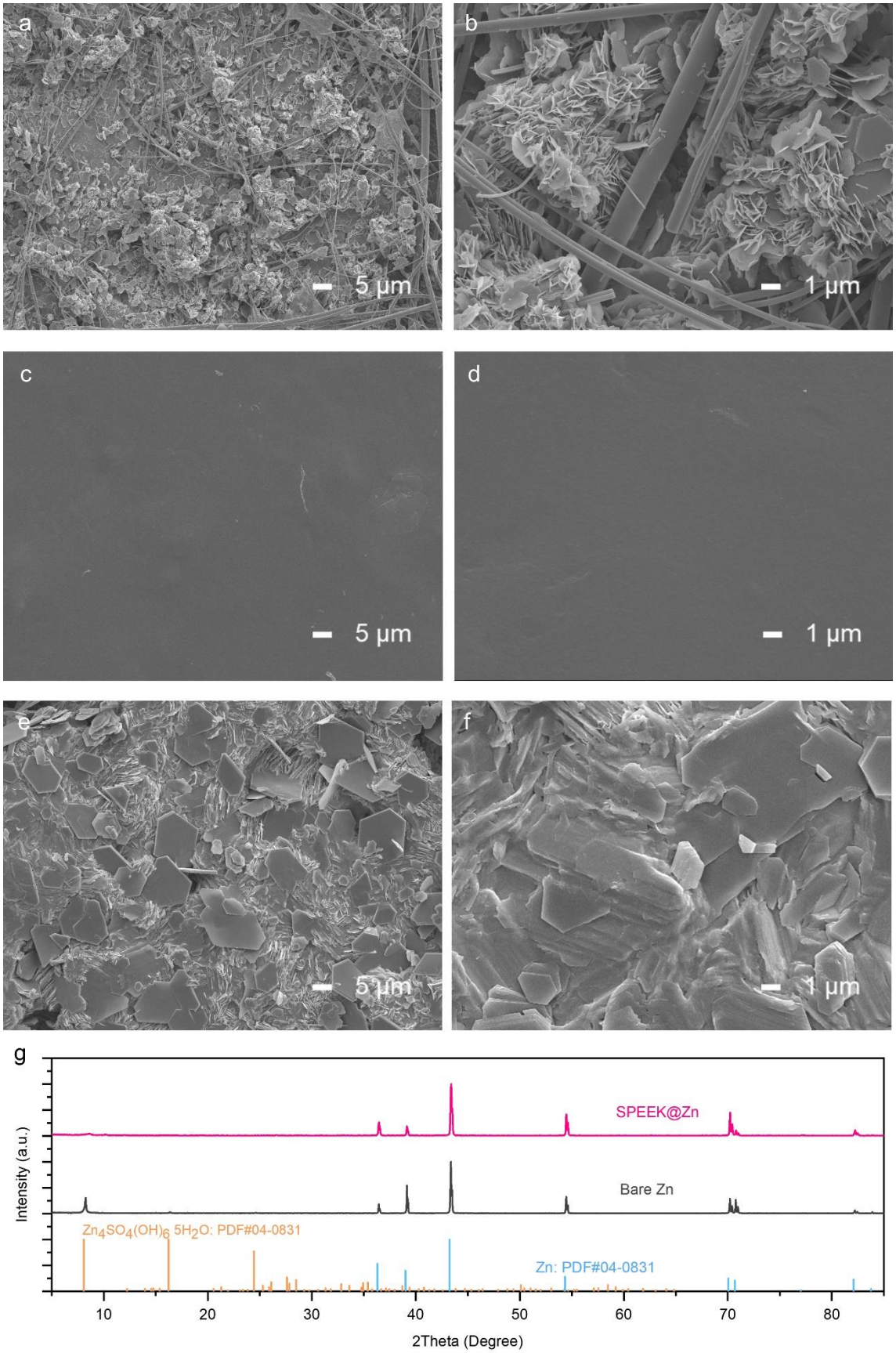

Figure 6. SEM images of (a, b) bare Zn electrode, (c, d) Zn@SPEEK electrode with SPEEK

SEI and (e, f) Zn@SPEEK electrode after tearing off the SPEEK SEI layer after 50 cycles at 5 mA cm^{-2} and 1 mAh cm^{-2}. (g) XRD patterns of bare Zn and Zn@SPEEK (after peeling off SPEEK SEI) electrode after 50 cycles.

To demonstrate the practical application of Zn@SPEEK anode, Zn–MnO_2 full cells incorporating a Zn@SPEEK anode and MnO_2/carbon nanotube (CNT) cathode were constructed and evaluated. The rate performance of the full cells with varying Zn anodes operating from 0.2 to 2 A g^{-1} are displayed in Figure 7a. The Zn@SPEEK electrode enable the battery to deliver a high discharge capacity of 280 mAh g^{-1} at 0.2 A g^{-1} and 127 mA h g^{-1} at 2 A g^{-1}, which are only 250 and 95 mA h g^{-1} for the cell with original Zn electrode. The charge-discharge voltage curves of the Zn-MnO_2 battery with bare Zn anode and Zn@SPEEK anode under various current densities from 0.2 to 2 A g^{-1} are displayed in Figure 7b. The cell with Zn@SPEEK anode shows a lower average charge plateau and higher average discharge plateau with higher coulombic efficiency which contributes to higher discharge capacity, showing the superior rate performance of Zn@SPEEK anode in full cell configuration. Apart from the rate capability, repeated long-term charge/discharge tests were conducted to evaluate the cycling stability of the Zn@SPEEK electrode, which is also of vital importance for real-world applications. First, cycling test of Zn-MnO_2 batteries was conducted at a small current density of 0.1 A g^{-1} to better study the effect of SPEEK SEI in inhibiting the side reactions with a long charge and discharge time. As presented in Figure 7c, with the protection of SPEEK SEI, the average CE of the first 40 cycles is improved from 97% to 99%, suggesting significantly improved reversibility of the Zn anode. The initial capacity of the cell with Zn@SPEEK is 294

mAh g^{-1}, which is higher than that with bare Zn anode (271 mAh g^{-1}). This is possibly owing to the severe side reactions between Zn and electrolyte, leading to the consumption of protons in the electrolyte, which as a result, lead to a lower initial capacity than that with a protected Zn anode. Furthermore, benefiting from the inhibited dendrite formation as well as side reactions, the cell with Zn@SPEEK delivers a capacity retention rate of 63% after 120 cycles (over 600 h), far exceeding the cell with bare Zn anode, which can only retain 35% of the initial capacity. Important cycle voltage curves are displayed in Figure S10. Remarkably, when cycled under a high current density of 1 A g^{-1}, the battery with Zn@SPEEK anode can still deliver a high discharge capacity and maintain a high capacity retention rate of 70% over 1000 cycles and over 60% after 2000 cycles. The charge/discharge curves at different cycles are shown in Figure S11. By comparison, the cell with the bare Zn anode suffers from fast decay from 165 to 56 mAh g^{-1} after only 1000 cycles, equivalent to a retention rate of as low as 34%, which is also reflected in the cycling voltage curves. These results demonstrate that the newly developed SPEEK SEI can effectively mitigate side reactions and dendrite growth of the Zn anode, thereby considerably boosting the cycle life of rechargeable Zn batteries.

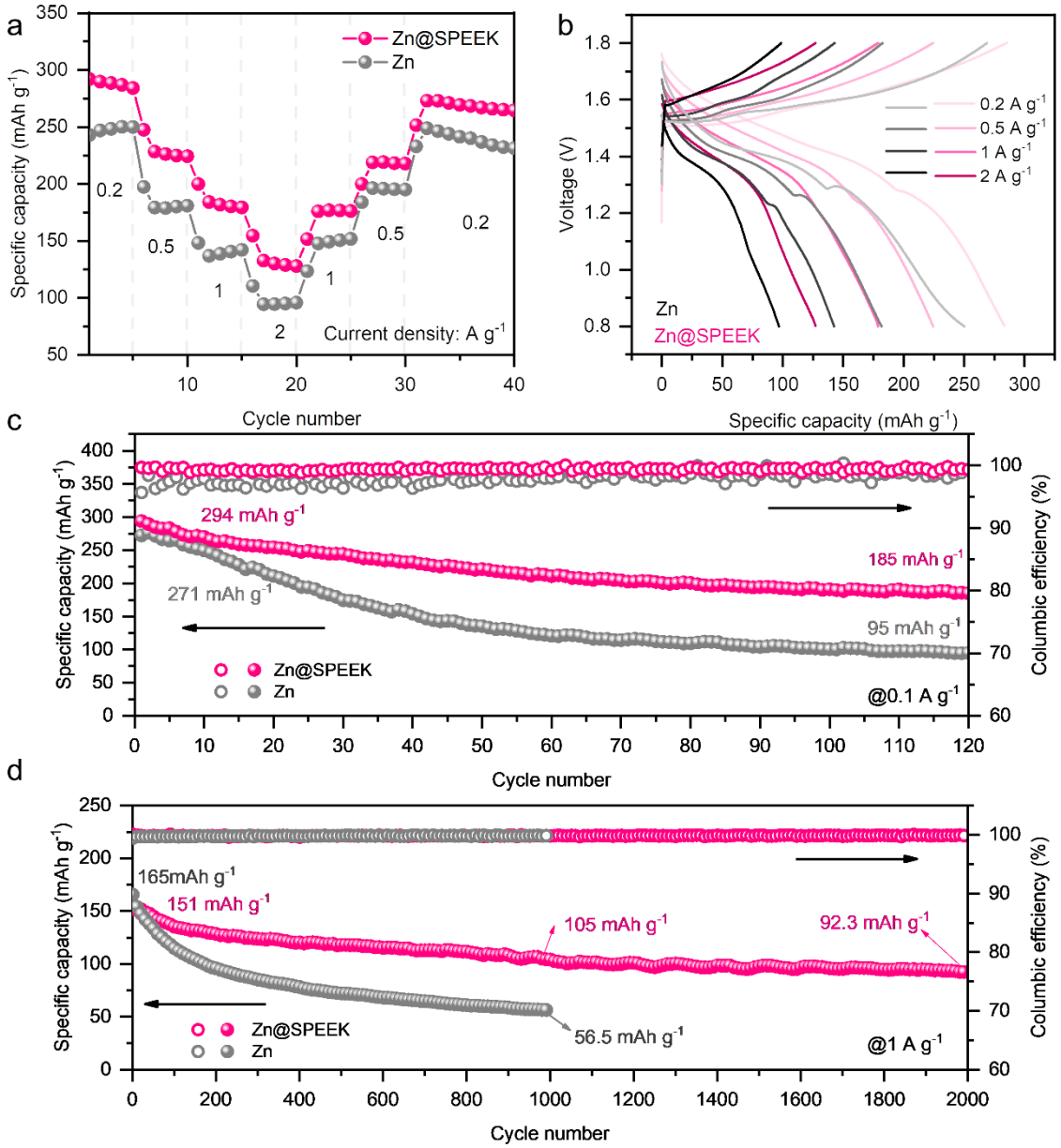

Figure 7. (a) Rate performance; (b) charge and discharge voltage profiles at different current densities; long-term cycling performance at (c) 0.1 A g^{-1} and (d) 1 A g^{-1} of Zn–MnO_2/CNT full batteries.

3 Conclusion

In summary, an ultra-thin de-solvation and anion-blocking artificial SEI made of a low-cost cation-conductive polymer, SPEEK, is successfully developed for highly reversible Zn anodes. It is demonstrated that the thin SPEEK layer with a high mechanical strength and good ionic

conductivity is capable of blocking water molecules and anions, facilitating the de-solvation kinetics and uniformizing the ionic flux, thus effectively inhibiting the side reactions and dendrite formation of Zn anode. As a consequence, the Zn@SPEEK enables a symmetric cell to achieve a stable cycling performance under both high current density and high areal capacity. More importantly, the Zn-MnO_2 full battery with the Zn@SPEEK anode displays a high average CE (99.0% at 0.1 A g^{-1}), an outstanding rate performance (127 mAh g^{-1} at 2 A g^{-1}) and a significantly improved capacity retention rate (70% after 1000 cycles at 1 A g^{-1}) during long-term cycling. This work opens up a new strategy for constructing an ionic conductive polymeric SEI toward stable, highly reversibly and dendrite-free Zn anodes.

4 Experimental

4.1 Synthesis of SPEEK

First, PEEK (VESTAKEEP, 4000P) was dried in vacuum at 100 ℃ for 12 h. After that, 5 g of PEEK was gradually added into 100 mL concentrated sulfuric acid (H_2SO_4, Sigma-Aldrich, 95-98%). The mixture was vigorously stirred and heated at 50 ℃ for 2.5 h. Then the sulfonation reaction was terminated by pouring the solution into ice-cold water. The precipitates were subsequently washed and filtered with deionized water until the pH became neutral. Finally, the resultants were completely dried in vacuum at 60 ℃ for at least 12 h. The degree of sulfonation (DS) for the synthesized SPEEK sample was measured to be 45.5% via titration.

4.2 Fabrication of Zn@SPEEK anode

The artificial SPEEK film coated on the surface of Zn foil was obtained via a spin-coating method. Specifically, the bare Zn foil was cleaned with diluted hydrochloric acid (HCl) and

ethanol to remove the oxidation layer and impurity on the surface. The as-prepared SPEEK powder was dissolved in dimethylacetamide (Sigma-Aldrich, 99%) to prepare a ~10 wt% SPEEK solution. Subsequently, the SPEEK was homogeneously coated on the fresh Zn foil using a spin-coater at a spin speed of 1000 rpm for 15 s.

Supporting Information

Preparation of MnO_2/CNT cathode; Materials and electrochemical characterizations; Rolling and twisting experiments; Immersion corrosion test; Hydrophilicity results; Ion transference number experiments; Ionic conductivity measurement; Mechanical strength of SPEEK; SEM, XRD and EDS mapping results.

In-situ observations of the Zn deposition on Zn (Video S1, 768× speed) and Zn@SPEEK (Video S2, 768× speed).

Acknowledgement

The work described in this paper was supported by the Research Grant Council Collaborative Research Fund of the Hong Kong Special Administrative Region, China (Project No. C5031-20G) and Natural Science Foundation of Guangdong Province (Grant No. 2021A1515011815).

Conflict of interest

The authors declare no conflicts of interest.

References

(1) Ibrahim, H.; Ilinca, A.; Perron, J. Energy Storage Systems-Characteristics and Comparisons. *Renew. Sustain. Energy Rev.* **2008**, *12*, 1221–1250.

(2) Evans, A.; Strezov, V.; Evans, T. J. Assessment of Utility Energy Storage Options for Increased Renewable Energy Penetration. *Renew. Sustain. Energy Rev.* **2012**, *16*, 4141–4147.

(3) Dunn, B.; Kamath, H.; Tarascon, J. M. Electrical Energy Storage for the Grid: A Battery of Choices. *Science.* **2011**, *334*, 928–935.

(4) Goodenough, J. B. Electrochemical Energy Storage in a Sustainable Modern Society. *Energy and Environmental Science*. Royal Society of Chemistry December 11, 2014, pp 14–18.

(5) Ao, H.; Zhao, Y.; Zhou, J.; Cai, W.; Zhang, X.; Zhu, Y.; Qian, Y. Rechargeable Aqueous Hybrid Ion Batteries: Developments and Prospects. *J. Mater. Chem. A* **2019**, *7*, 18708–18734.

(6) Yuan, D.; Zhao, J.; Manalastas, W.; Kumar, S.; Srinivasan, M. Emerging Rechargeable Aqueous Aluminum Ion Battery: Status, Challenges, and Outlooks. *Nano Mater. Sci.* **2020**, *2*, 248–263.

(7) Liu, T.; Cheng, X.; Yu, H.; Zhu, H.; Peng, N.; Zheng, R.; Zhang, J.; Shui, M.; Cui, Y.; Shu, J. An Overview and Future Perspectives of Aqueous Rechargeable Polyvalent Ion Batteries. *Energy Storage Mater.* **2019**, *18*, 68–91.

(8) Yao, Y.; Wang, Z.; Li, Z.; Lu, Y.-C. A Dendrite-Free Tin Anode for High-Energy Aqueous Redox Flow Batteries. *Adv. Mater.* **2021**, *33*, 2008095.

(9) Lei, J.; Yao, Y.; Wang, Z.; Lu, Y.-C. Towards High-Areal-Capacity Aqueous Zinc–Manganese Batteries: Promoting MnO2 Dissolution by Redox Mediators. *Energy Environ. Sci.* **2021**, *14*, 4418–4426.

(10) Li, H.; Ma, L.; Han, C.; Wang, Z.; Liu, Z.; Tang, Z.; Zhi, C. Advanced Rechargeable

Zinc-Based Batteries: Recent Progress and Future Perspectives. *Nano Energy* **2019**, *62*, 550–587.

(11) Li, Q.; Zhao, Y.; Mo, F.; Wang, D.; Yang, Q.; Huang, Z.; Liang, G.; Chen, A.; Zhi, C. Dendrites Issues and Advances in Zn Anode for Aqueous Rechargeable Zn-based Batteries. *EcoMat* **2020**, *2*, e12035.

(12) Li, C.; Xie, X.; Liang, S.; Zhou, J. Issues and Future Perspective on Zinc Metal Anode for Rechargeable Aqueous Zinc-ion Batteries. *Energy Environ. Mater.* **2020**, *3*, 146–159.

(13) Hao, J.; Li, X.; Zeng, X.; Li, D.; Mao, J.; Guo, Z. Deeply Understanding the Zn Anode Behaviour and Corresponding Improvement Strategies in Different Aqueous Zn-Based Batteries. *Energy Environ. Sci.* **2020**, *13*, 3917–3949.

(14) Fu, J.; Liang, R.; Liu, G.; Yu, A.; Bai, Z.; Yang, L.; Chen, Z. Recent Progress in Electrically Rechargeable Zinc–Air Batteries. *Adv. Mater.* **2019**, *31*, 1805230.

(15) Fu, J.; Cano, Z. P.; Park, M. G.; Yu, A.; Fowler, M.; Chen, Z. Electrically Rechargeable Zinc–Air Batteries: Progress, Challenges, and Perspectives. *Adv. Mater.* **2017**, *29*.

(16) Chen, P.; Wu, Y.; Zhang, Y.; Wu, T. H.; Ma, Y.; Pelkowski, C.; Yang, H.; Zhang, Y.; Hu, X.; Liu, N. A Deeply Rechargeable Zinc Anode with Pomegranate-Inspired Nanostructure for High-Energy Aqueous Batteries. *J. Mater. Chem. A* **2018**, *6*, 21933–21940.

(17) Wu, Y.; Zhang, Y.; Ma, Y.; Howe, J. D.; Yang, H.; Chen, P.; Aluri, S.; Liu, N. Ion-Sieving Carbon Nanoshells for Deeply Rechargeable Zn-Based Aqueous Batteries. *Adv. Energy Mater.* **2018**, *8*.

(18) Xu, C.; Li, B.; Du, H.; Kang, F. Energetic Zinc Ion Chemistry: The Rechargeable Zinc Ion Battery. *Angew. Chemie* **2012**, *124*, 957–959.

(19) Zhang, N.; Cheng, F.; Liu, J.; Wang, L.; Long, X.; Liu, X.; Li, F.; Chen, J. Rechargeable Aqueous Zinc-Manganese Dioxide Batteries with High Energy and Power Densities. *Nat. Commun.* **2017**, *8*, 1–9.

(20) Kundu, D.; Adams, B. D.; Duffort, V.; Vajargah, S. H.; Nazar, L. F. A High-Capacity and Long-Life Aqueous Rechargeable Zinc Battery Using a Metal Oxide Intercalation Cathode. *Nat. Energy* **2016**, *1*, 1–8.

(21) Pan, H.; Shao, Y.; Yan, P.; Cheng, Y.; Han, K. S.; Nie, Z.; Wang, C.; Yang, J.; Li, X.; Bhattacharya, P.; Mueller, K. T.; Liu, J. Reversible Aqueous Zinc/Manganese Oxide Energy Storage from Conversion Reactions. *Nat. Energy* **2016**, *1*, 16039.

(22) Wang, J.; Yang, Y.; Zhang, Y.; Li, Y.; Sun, R.; Wang, Z.; Wang, H. Strategies towards the Challenges of Zinc Metal Anode in Rechargeable Aqueous Zinc Ion Batteries. *Energy Storage Mater.* **2021**, *35*, 19–46.

(23) Wang, T.; Li, C.; Xie, X.; Lu, B.; He, Z.; Liang, S.; Zhou, J. Anode Materials for Aqueous Zinc Ion Batteries: Mechanisms, Properties, and Perspectives. *ACS Nano*. American Chemical Society December 22, 2020, pp 16321–16347.

(24) Tian, Y.; An, Y.; Liu, C.; Xiong, S.; Feng, J.; Qian, Y. Reversible Zinc-Based Anodes Enabled by Zincophilic Antimony Engineered MXene for Stable and Dendrite-Free Aqueous Zinc Batteries. *Energy Storage Mater.* **2021**, *41*, 343–353.

(25) Tian, Y.; An, Y.; Wei, C.; Xi, B.; Xiong, S.; Feng, J.; Qian, Y. Flexible and Free-

Standing Ti3C2Tx MXene@Zn Paper for Dendrite-Free Aqueous Zinc Metal Batteries and Nonaqueous Lithium Metal Batteries. *ACS Nano* **2019**, *13*, 11676–11685.

(26) An, Y.; Tian, Y.; Xiong, S.; Feng, J.; Qian, Y. Scalable and Controllable Synthesis of Interface-Engineered Nanoporous Host for Dendrite-Free and High Rate Zinc Metal Batteries. *ACS Nano* **2021**, *15*, 11828–11842.

(27) Jian, Q.; Guo, Z.; Zhang, L.; Wu, M.; Zhao, T. A Hierarchical Porous Tin Host for Dendrite-Free, Highly Reversible Zinc Anodes. *Chem. Eng. J.* **2021**, *425*, 130643.

(28) Wang, C.; Zhu, G.; Liu, P.; Chen, Q. Monolithic Nanoporous Zn Anode for Rechargeable Alkaline Batteries. *ACS Nano* **2020**, *14*, 2404–2411.

(29) Guo, W.; Cong, Z.; Guo, Z.; Chang, C.; Liang, X.; Liu, Y.; Hu, W.; Pu, X. Dendrite-Free Zn Anode with Dual Channel 3D Porous Frameworks for Rechargeable Zn Batteries. *Energy Storage Mater.* **2020**, *30*, 104–112.

(30) Parker, J. F.; Chervin, C. N.; Pala, I. R.; Machler, M.; Burz, M. F.; Long, J. W.; Rolison, D. R. Rechargeable Nickel-3D Zinc Batteries: An Energy-Dense, Safer Alternative to Lithium-Ion. *Science (80-.).* **2017**, *356*, 415–418.

(31) Parker, J. F.; Chervin, C. N.; Nelson, E. S.; Rolison, D. R.; Long, J. W. Wiring Zinc in Three Dimensions Re-Writes Battery Performance - Dendrite-Free Cycling. *Energy Environ. Sci.* **2014**, *7*, 1117–1124.

(32) Chamoun, M.; Hertzberg, B. J.; Gupta, T.; Davies, D.; Bhadra, S.; Tassell, B. Van; Erdonmez, C.; Steingart, D. A. Hyper-Dendritic Nanoporous Zinc Foam Anodes. *NPG Asia Mater.* **2015**, *7*, 178.

(33) Hao, J.; Li, B.; Li, X.; Zeng, X.; Zhang, S.; Yang, F.; Liu, S.; Li, D.; Wu, C.; Guo, Z. An In-Depth Study of Zn Metal Surface Chemistry for Advanced Aqueous Zn-Ion Batteries. *Adv. Mater.* **2020**, *32*, 2003021.

(34) Zhao, K.; Wang, C.; Yu, Y.; Yan, M.; Wei, Q.; He, P.; Dong, Y.; Zhang, Z.; Wang, X.; Mai, L. Ultrathin Surface Coating Enables Stabilized Zinc Metal Anode. *Adv. Mater. Interfaces* **2018**, *5*, 1800848.

(35) Kang, L.; Cui, M.; Jiang, F.; Gao, Y.; Luo, H.; Liu, J.; Liang, W.; Zhi, C. Nanoporous $CaCO_3$ Coatings Enabled Uniform Zn Stripping/Plating for Long-Life Zinc Rechargeable Aqueous Batteries. *Adv. Energy Mater.* **2018**, *8*, 1801090.

(36) He, H.; Tong, H.; Song, X.; Song, X.; Liu, J. Highly Stable Zn Metal Anodes Enabled by Atomic Layer Deposited Al2O3 Coating for Aqueous Zinc-Ion Batteries. *J. Mater. Chem. A* **2020**, *8*, 7836–7846.

(37) Jian, Q.; Wan, Y.; Sun, J.; Wu, M.; Zhao, T. A Dendrite-Free Zinc Anode for Rechargeable Aqueous Batteries. *J. Mater. Chem. A* **2020**, *8*, 20175–20184.

(38) Cao, P.; Zhou, X.; Wei, A.; Meng, Q.; Ye, H.; Liu, W.; Tang, J.; Yang, J. Fast-Charging and Ultrahigh-Capacity Zinc Metal Anode for High-Performance Aqueous Zinc-Ion Batteries. *Adv. Funct. Mater.* **2021**, *31*, 2100398.

(39) Wu, B.; Wu, Y.; Lu, Z.; Zhang, J.; Han, N.; Wang, Y.; Li, X. M.; Lin, M.; Zeng, L. A Cation Selective Separator Induced Cathode Protective Layer and Regulated Zinc Deposition for Zinc Ion Batteries. *J. Mater. Chem. A* **2021**, *9*, 4734–4743.

(40) Yuan, D.; Manalastas, W.; Zhang, L.; Chan, J. J.; Meng, S.; Chen, Y.; Srinivasan, M.

Lignin@Nafion Membranes Forming Zn Solid–Electrolyte Interfaces Enhance the Cycle Life for Rechargeable Zinc-Ion Batteries. *ChemSusChem* **2019**, *12*, 4889–4900.

(41) Wang, F.; Borodin, O.; Gao, T.; Fan, X.; Sun, W.; Han, F.; Faraone, A.; Dura, J. A.; Xu, K.; Wang, C. Highly Reversible Zinc Metal Anode for Aqueous Batteries. *Nat. Mater.* **2018**, *17*, 543–549.

(42) Yang, H.; Chang, Z.; Qiao, Y.; Deng, H.; Mu, X.; He, P.; Zhou, H. Constructing a Super-Saturated Electrolyte Front Surface for Stable Rechargeable Aqueous Zinc Batteries. *Angew. Chemie Int. Ed.* **2020**, *59*, 9377–9381.

(43) Zhang, Q.; Ma, Y.; Lu, Y.; Li, L.; Wan, F.; Zhang, K.; Chen, J. Modulating Electrolyte Structure for Ultralow Temperature Aqueous Zinc Batteries. *Nat. Commun.* **2020**, *11*, 1–10.

(44) Hou, Z.; Tan, H.; Gao, Y.; Li, M.; Lu, Z.; Zhang, B. Tailoring Desolvation Kinetics Enables Stable Zinc Metal Anodes. *J. Mater. Chem. A* **2020**, *8*, 19367–19374.

(45) Jian, Q. P.; Wu, M. C.; Jiang, H. R.; Lin, Y. K.; Zhao, T. S. A Trifunctional Electrolyte for High-Performance Zinc-Iodine Flow Batteries. *J. Power Sources* **2021**, *484*, 229238.

(46) Guo, X.; Zhang, Z.; Li, J.; Luo, N.; Chai, G. L.; Miller, T. S.; Lai, F.; Shearing, P.; Brett, D. J. L.; Han, D.; Weng, Z.; He, G.; Parkin, I. P. Alleviation of Dendrite Formation on Zinc Anodes via Electrolyte Additives. *ACS Energy Lett.* **2021**, *31*, 395–403.

(47) Wu, Y.; Zhang, Y.; Ma, Y.; Howe, J. D.; Yang, H.; Chen, P.; Aluri, S.; Liu, N. Ion-Sieving Carbon Nanoshells for Deeply Rechargeable Zn-Based Aqueous Batteries. *Adv. Energy Mater.* **2018**, *8*, 1–7.

(48) Zhao, Z.; Zhao, J.; Hu, Z.; Li, J.; Li, J.; Zhang, Y.; Wang, C.; Cui, G. Long-Life and

Deeply Rechargeable Aqueous Zn Anodes Enabled by a Multifunctional Brightener-Inspired Interphase. *Energy Environ. Sci.* **2019**, *12*, 1938–1949.

(49) Cao, Z.; Zhu, X.; Xu, D.; Dong, P.; Chee, M. O. L.; Li, X.; Zhu, K.; Ye, M.; Shen, J. Eliminating Zn Dendrites by Commercial Cyanoacrylate Adhesive for Zinc Ion Battery. *Energy Storage Mater.* **2021**, *36*, 132–138.

(50) Cui, Y.; Zhao, Q.; Wu, X.; Chen, X.; Yang, J.; Wang, Y.; Qin, R.; Ding, S.; Song, Y.; Wu, J.; Yang, K.; Wang, Z.; Mei, Z.; Song, Z.; Wu, H.; Jiang, Z.; Qian, G.; Yang, L.; Pan, F. An Interface-Bridged Organic–Inorganic Layer That Suppresses Dendrite Formation and Side Reactions for Ultra-Long-Life Aqueous Zinc Metal Anodes. *Angew. Chemie* **2020**, *132*, ange.202005472.

(51) Jiang, Y.; Hao, J.; Hou, M.; Hong, S.; Song, W.; Yi, B.; Shao, Z. A Novel Porous Sulfonated Poly(Ether Ether Ketone)-Based Multi-Layer Composite Membrane for Proton Exchange Membrane Fuel Cell Application. *Sustain. Energy Fuels* **2017**, *1*, 1405–1413.

(52) Gong, X.; He, G.; Wu, Y.; Zhang, S.; Chen, B.; Dai, Y.; Wu, X. Aligned Electrospun Nanofibers as Proton Conductive Channels through Thickness of Sulfonated Poly (Phthalazinone Ether Sulfone Ketone) Proton Exchange Membranes. *J. Power Sources* **2017**, *358*, 134–141.

(53) Dai, W.; Shen, Y.; Li, Z.; Yu, L.; Xi, J.; Qiu, X. SPEEK/Graphene Oxide Nanocomposite Membranes with Superior Cyclability for Highly Efficient Vanadium Redox Flow Battery. *J. Mater. Chem. A* **2014**, *2*, 12423–12432.

(54) Montero, J. F. D.; Barbosa, L. C. A.; Pereira, U. A.; Barra, G. M.; Fredel, M. C.;

Benfatti, C. A. M.; Magini, R. S.; Pimenta, A. L.; Souza, J. C. M. Chemical, Microscopic, and Microbiological Analysis of a Functionalized Poly-Ether-Ether-Ketone-Embedding Antibiofilm Compounds. *J. Biomed. Mater. Res. Part A* **2016**, *104*, 3015–3020.

(55) Hosseinabadi, P.; Hooshyari, K.; Javanbakht, M.; Enhessari, M. Synthesis and Optimization of Nanocomposite Membranes Based on SPEEK and Perovskite Nanoparticles for Polymer Electrolyte Membrane Fuel Cells. *New J. Chem.* **2019**, *43*, 16232–16245.

(56) Hao, J.; Li, X.; Zhang, S.; Yang, F.; Zeng, X.; Zhang, S.; Bo, G.; Wang, C.; Guo, Z. Designing Dendrite-Free Zinc Anodes for Advanced Aqueous Zinc Batteries. *Adv. Funct. Mater.* **2020**, *30*, 2001263.

(57) Hao, J.; Yuan, L.; Ye, C.; Chao, D.; Davey, K.; Guo, Z.; Qiao, S. Z. Boosting Zinc Electrode Reversibility in Aqueous Electrolytes by Using Low-Cost Antisolvents. *Angew. Chemie - Int. Ed.* **2021**, *60*, 7366–7375.

(58) Cai, Z.; Ou, Y.; Wang, J.; Xiao, R.; Fu, L.; Yuan, Z.; Zhan, R.; Sun, Y. Chemically Resistant Cu–Zn/Zn Composite Anode for Long Cycling Aqueous Batteries. *Energy Storage Mater.* **2020**, *27*, 205–211.

(59) Zhao, Z.; Zhao, J.; Hu, Z.; Li, J.; Li, J.; Zhang, Y.; Wang, C.; Cui, G. Long-Life and Deeply Rechargeable Aqueous Zn Anodes Enabled by a Multifunctional Brightener-Inspired Interphase. *Energy Environ. Sci.* **2019**, *12*, 1938–1949.

(60) Bayaguud, A.; Luo, X.; Fu, Y.; Zhu, C. Cationic Surfactant-Type Electrolyte Additive Enables Three-Dimensional Dendrite-Free Zinc Anode for Stable Zinc-Ion Batteries. *ACS Energy Lett.* **2020**, *5*, 3012–3020.

(61) Lin, C. E.; Zhang, H.; Song, Y. Z.; Zhang, Y.; Yuan, J. J.; Zhu, B. K. Carboxylated Polyimide Separator with Excellent Lithium Ion Transport Properties for a High-Power Density Lithium-Ion Battery. *J. Mater. Chem. A* **2018**, *6*, 991–998.

(62) Komaba, S.; Ozeki, T.; Okushi, K. Functional Interface of Polymer Modified Graphite Anode. *J. Power Sources* **2009**, *189*, 197–203.

(63) Jiang, C.; Gu, Y.; Tang, M.; Chen, Y.; Wu, Y.; Ma, J.; Wang, C.; Hu, W. Toward Stable Lithium Plating/Stripping by Successive Desolvation and Exclusive Transport of Li Ions. *ACS Appl. Mater. Interfaces* **2020**, *12*, 10461–10470.

(64) Purser, E. P.; Stokes, R. H. Transference Numbers in Aqueous Solutions of Zinc Sulfate. *J. Am. Chem. Soc.* **1951**, *73*, 5650–5652.

(65) Stokes, R. H. An Alternative Computation of the Transference Numbers in Zinc Sulfate Solutions. *J. Am. Chem. Soc.* **1955**, *77*, 3219.

(66) Ma, L.; Schroeder, M. A.; Pollard, T. P.; Borodin, O.; Ding, M. S.; Sun, R.; Cao, L.; Ho, J.; Baker, D. R.; Wang, C.; Xu, K. Critical Factors Dictating Reversibility of the Zinc Metal Anode. *Energy Environ. Mater.* **2020**, *3*, 516–521.

(67) Ma, L.; Schroeder, M. A.; Borodin, O.; Pollard, T. P.; Ding, M. S.; Wang, C.; Xu, K. Realizing High Zinc Reversibility in Rechargeable Batteries. *Nat. Energy* **2020**, *5*, 743–749.

(68) Zhou, M.; Guo, S.; Li, J.; Luo, X.; Liu, Z.; Zhang, T.; Cao, X.; Long, M.; Lu, B.; Pan, A.; Fang, G.; Zhou, J.; Liang, S. Surface-Preferred Crystal Plane for a Stable and Reversible Zinc Anode. *Adv. Mater.* **2021**, 2100187.

(69) Zhang, X.; Li, J.; Liu, D.; Liu, M.; Zhou, T.; Qi, K.; Shi, L.; Zhu, Y.; Qian, Y. Ultra-

Long-Life and Highly Reversible Zn Metal Anodes Enabled by a Desolvation and Deanionization Interface Layer. *Energy Environ. Sci.* **2021**, *14*, 3120.

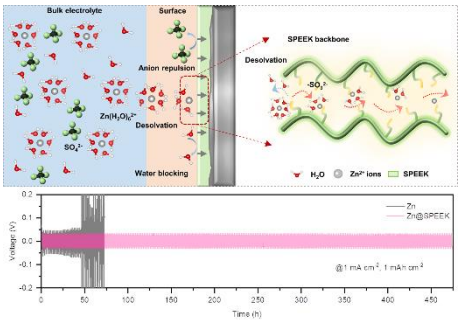

Table of Contents